Condensed Matter and Interphases

Original articles

Synthesis, structure, and photo-Fenton activity of PrFeO$_3$-TiO$_2$ mesoporous nanocomposites

A. S. Seroglazova[1,2]✉, M. I. Chebanenko[2], V. I. Popkov[2]

[1]*Saint-Petersburg State Institute of Technology,
26 Moskovsky pr., Saint Petersburg 190013, Russian Federation*

[2]*Ioffe Institute,
26 Politekhnicheskaya str., Saint Petersburg 194021, Russian Federation*

Abstract

Porous nanocomposites based on PrFeO$_3$-TiO$_2$ were synthesized using the glycine-nitrate combustion method with different values of mass content of TiO$_2$ (0–7.5 %) and subsequent heat treatment in air. The results of X-ray phase analysis and Raman spectroscopy confirmed the presence of ultradispersed TiO$_2$, structurally close to that of anatase. The morphology, specific surface area, and porous structure of the obtained powders were characterized by scanning electron microscopy and adsorption-structural analysis, the results of which showed that the samples had a foam-like mesoporous structure. The specific surface area and the average pore size were in the ranges of 7.6–17.8 m^2/g and 7.2–15.2 nm, respectively, and varied depending on the TiO$_2$ content. The optical properties of the nanocomposites were studied by UV-visible diffuse reflection spectroscopy, the energy of the band gap was calculated as 2.11–2.26 eV. The photocatalytic activity of PrFeO$_3$-TiO$_2$ nanocomposites was investigated in the process of photo-Fenton-like degradation of methyl violet under the action of visible light. It was shown that the maximum reaction rate constant was 0.095 min^{-1}, which is ten times higher than the value for the known orthoferrite-based analogs. The obtained photocatalysts were also characterized by their high cyclic stability. Based on the studies carried out, the obtained porous PrFeO$_3$-TiO$_2$ nanocomposites can be considered to be a promising basis for photocatalysts applied in advanced oxidative processes of aqueous media purification from organic pollutants.

Keywords: Solution-combustion synthesis; Praseodymium orthoferrite; Titanium Oxide; Nanocomposites; Photocatalysts; Fenton-like reactions

✉ Anna S. Seroglazova, e-mail: annaseroglazova@yandex.ru

Condensed Matter and Interphases / Конденсированные среды и межфазные границы   2021;23(4): 548–560

A. S. Seroglazova et al.   Synthesis, structure, and photo-Fenton activity of PrFeO$_3$-TiO$_2$...

1. Introduction

Most industries for the manufacture of plastics, fabrics, paper, and rubber use various dyes and organic substances, leading not only to environmental pollution but also to the development of various diseases in humans, since they are often carcinogenic and/or highly toxic compounds. Traditional methods of removing organic dyes such as adsorption, filtration, ozonizing filtration, electrochemistry, used in modern industries, are quite effective, but still do not achieve a complete decomposition of the organic dyes due to their complex aromatic structure and resistance to various environmental factors, including oxidation. Therefore, there is an urgent need for the development of an alternative, for example, photocatalytic methods of water purification using environmentally friendly photocatalysts, which make it possible to effectively destroy toxic organic substances under the action of visible light.

Orthoferrites are complex oxides based on rare earth elements (REE) and iron with the general chemical formula of RFeO$_3$ (R = Sc, Y, Ln), having a distorted perovskite-like structure with the Pbnm/Pnma space group [1–4]. Recently, there has been an increased interest in the study of REE orthoferrites due to their unique physical and chemical properties, which opens a wide range of possibilities for their practical application as a basis for new functional materials [5–8]. In addition, the structural, electromagnetic, and catalytic properties of REE orthoferrites make it possible to use them in the production of ceramics, magnetic devices, gas sensors, and magnetically controlled photocatalysts [9–11].

Earlier, various methods of synthesis were used to obtain nanocrystalline orthoferrites of rare earth elements: microwave, hydrothermal, sol-gel, co-precipitation, and others [1,12–15]. Most of these methods are labor-intensive and energy-consuming and do not always allow the control of such important parameters as particle size, shape, morphology, and structure, which determine the functional properties of REE orthoferrites. However, as was shown earlier in works [16–18], the solution combustion mthod is free from these drawbacks and allows varying the porous structure of nanoparticle aggregates, and thereby controlling the functional properties of the obtained materials based on REE orthoferrites. The two-stage synthesis of REE orthoferrites with the amorphous combustion products and their further thermal treatment to obtain pure product is particularly promising. Powders obtained by this method are characterized by their porous structure, foamy morphology, and developed surface. The latter is an important factor in the development of photocatalytic materials [19].

Among the most promising photocatalysts based on REE orthoferrites, PrFeO$_3$ stands out, which has an unusually high activity under the action of visible light [20]. Interest in such materials is caused by the possibility of their participation in heterogeneous Fenton-like processes occurring in an aqueous-organic solution. The mechanism of Fenton-like oxidation consists of the formation of powerful oxidizing hydroxyl radicals (OH·) during the reversible transition from Fe^{2+} to Fe^{3+} under the action of visible light, which makes it possible to achieve the highly efficient decomposition and oxidation of organic pollutants [21–23]. Despite the high catalytic activity, reverse recombination processes significantly impair the photocatalytic activity of such materials, including PrFeO$_3$. As reported in [19], the reverse recombination processes can be suppressed through the creation of a heterojunction structure during the transition from PrFeO$_3$ to a composite based on it. For several simple oxides, it has been shown that an improvement in the photocatalytic properties can be achieved by adding a second component, due to the presence of which the transfer of charge carriers becomes possible immediately after the formation of an electron-hole pair under the action of irradiation [24–28]. Thus, the transition to heterostructures based on nanocomposites of rare-earth elements and other oxides is one of the most effective strategies for suppressing electron-hole recombination. In the presented work, TiO$_2$ was chosen to improve the photocatalytic characteristics of PrFeO$_3$, which, according to modern concepts, should lead to a drop in recombination. In addition, TiO$_2$ is an active, stable, and environmentally friendly photocatalyst in the near-UV region with a strong oxidizing ability [29–31]. Interest in studying its catalytic properties when paired with PrFeO$_3$ is also associated with the relatively large band

Condensed Matter and Interphases / Конденсированные среды и межфазные границы   2021;23(4): 548–560

A. S. Seroglazova et al.   Synthesis, structure, and photo-Fenton activity of PrFeO₃-TiO₂...

gap of TiO$_2$ and the high intrinsic generation of electron-hole pairs.

This paper is dedicated to obtaining PrFeO$_3$-TiO$_2$ nanocomposite materials by the method of solution combustion with different values of TiO$_2$ content (0-7.5 wt%). The obtained samples were studied using a wide range of physicochemical methods of analysis, allowing a detailed study of their structure, morphology, magnetic and optical properties, etc. Photocatalytic properties were studied using the example of Fenton-like oxidation of methyl violet (MV) under the action of visible light. The data obtained were compared with the results of photocatalytic studies of pure PrFeO$_3$ and other REE orthoferrites. PrFeO$_3$-TiO$_2$ nanocomposite materials demonstrated a significant increase in the efficiency of MV photocatalytic oxidation. Thus, the obtained powders can be used in modern advanced oxidative processes for the purification of contaminated aqueous media.

2. Materials and methods

2.1. Preparation of the titanyl nitrate (TiO(NO$_3$)$_2$) solution

The synthesis of nanocomposite powders based on PrFeO$_3$-TiO$_2$ included the preliminary preparation of titanyl nitrate TiO(NO$_3$)$_2$ from titanium tetrachloride TiCl$_4$ by hydrolysis. For this, distilled water was added to 20 ml of TiCl$_4$ with constant stirring until a white precipitate of TiO(OH)$_2$ was formed, followed by its complete dissolution in concentrated nitric acid (HNO$_3$).

2.2. Synthesis of PrFeO$_3$-TiO$_2$ nanocomposites

PrFeO$_3$-TiO$_2$ nanocomposites were prepared by the solution combustion method. To prepare the reaction mixture, we used the nitrates of the corresponding metals, Pr(NO$_3$)$_3$·6H$_2$O and Fe(NO$_3$)$_3$·9H$_2$O. Glycine with a glycine-nitrate ratio G/N = 2.0 was used as a fuel.

During the synthesis, iron (III) and praseodymium nitrates, as well as glycine, were dissolved in a small amount of distilled water, followed by the addition of a titanyl nitrate solution TiO(NO$_3$)$_2$. The resulting reaction mixture was stirred until the nitrates and glycine were completely dissolved. The reaction solution prepared in this way was heated in a sand bath until the water evaporated and the reaction

mixture ignited. As a result, porous brown powders were formed. Similarly, pure PrFeO$_3$ was synthesized, as well as a series of PrFeO$_3$-TiO$_2$ nanocomposite powders with different mass ratios of PrFeO$_3$:TiO$_2$ = 100:0, 97.5:2.5, 95:5, and 92.5:7.5%, which were then heat-treated at 700 °C for 1 hour in the air to remove unreacted impurities and form crystalline praseodymium orthoferrite from amorphous combustion products.

2.3. Physico-chemical characterization

The elemental composition and morphology of the synthesized samples were studied by energy-dispersive X-ray spectroscopy (EDS) and scanning electron microscopy (SEM) using a Tescan Vega 3 SBH scanning electron microscope.

To determine the phase composition of the samples, X-ray phase analysis was carried out on a Rigaku SmartLab X-ray powder diffractometer in the range of Bragg angles (2θ) from 20° to 60°. Qualitative X-ray phase analysis was performed using the ICSD database. Based on the broadening of the X-ray diffraction lines, the average crystallite size was calculated using the Scherrer formula:

$$D = \frac{k\lambda}{\beta \cos\theta}$$

where k – shape factor, equal to 0.94; λ – X-ray wavelength (Cu$K\alpha$ = 0.15406 nm); β – line broadening at half the maximum in radians; θ – Bragg's angle in radians.

The structural features of the nanocomposites were studied using Raman spectroscopy (excitation wavelength λ = 532 nm) on a SINTERRA Raman microscope.

The specific surface of the samples, pore volume, and pore size distribution were determined by adsorption-structural analysis (ASA) using a Micromeritics ASAP 2020. Sorption-desorption isotherms were obtained at a liquid nitrogen temperature of 77 K.

Diffuse reflectance spectra (DRS) were measured with an Avaspec-ULS2048 spectrometer equipped with an AvaSphere-30-Refl integrating sphere.

2.4. Photocatalytic measurements

The photocatalytic activity of the synthesized samples was estimated during the photocatalytic

Condensed Matter and Interphases / Конденсированные среды и межфазные границы 2021;23(4): 548–560

A. S. Seroglazova et al.   Synthesis, structure, and photo-Fenton activity of PrFeO$_3$-TiO$_2$...

degradation of methyl violet (MV) under the action of visible light. The dye concentration was measured using a Shimadzu UV1600 spectrophotometer. Two 100W xenon lamps with a UV filter of $\lambda \geqslant 420$ nm were used as a light source. The oxidation process was carried out in an experimental setup in the form of an insulated box, which included a 50 ml beaker, a magnetic stirrer, and lamps.

The first part of the experiment consisted in determining the most efficient catalyst among the samples PrFeO$_3$, PrFeO$_3$-TiO$_2$ 2.5%, PrFeO$_3$-TiO$_2$ 5%, PrFeO$_3$-TiO$_2$ 7.5%. For this, colloidal solutions of the corresponding nanopowders with a concentration of 0.5 g/L were preliminarily prepared. Then, 12.5 ml of a colloidal solution containing the catalyst, 0.6 ml of methyl violet (C = 1 g/L) and 6 ml of hydrogen peroxide (C = 1 mol/L), and 5.9 ml of distilled water were added to each of the four cuvettes. The final concentrations of these components in the resulting 25 ml volume were 0.25 g/L, 0.0232 g/L, and 0.24 mol/L, respectively. Before the start of the photocatalytic experiment, the solutions were stirred in the dark for 30 minutes to establish adsorption equilibrium. After this time, the solutions were irradiated with visible light with continuous stirring for 15 minutes. Then, 5 ml samples were taken from each solution to determine the concentration of the dye. Methyl violet removal efficiency was evaluated using the formula:

$$\text{Rem. Eff.} = \frac{C_0 - C}{C_0} \cdot 100\,\%,$$

where C_0 – initial dye concentration, C – final dye concentration after Fenton-like oxidation.

After the determination of the most active photocatalyst (PrFeO$_3$-TiO$_2$ 5%), the corresponding kinetic parameters of the photo-Fenton-like oxidation of methyl violet were studied. For this, 25 ml of a solution containing 12.5 ml of catalyst (C = 0.25 g/L), 1.2 ml of methyl violet (C = 0.0464 g/L), 6 ml of H$_2$O$_2$ (C = 0.24 mol/L), and 4.1 ml of H$_2$O were prepared. With constant stirring, the solution was irradiated for 15 minutes with a sample taken every 3 minutes to obtain the dependence of the efficiency of dye removal on the duration of irradiation.

In the final part of the experiment, the cyclic activity of the nanocomposite photocatalyst PrFeO$_3$-TiO$_2$ 5% was studied. As in the second experiment, a solution was prepared with the same concentrations of catalyst, dye, and hydrogen peroxide, which was irradiated for 15 minutes with constant stirring with sampling every 3 minutes. After 15 minutes, the final concentration of the decolorized dye was measured. Based on the obtained values of the final concentration MV, add the required volume of the dye to the initial solution so that its concentration becomes the same (C = 0.0464 g/L). Then this procedure was repeated.

3. Results and discussion

3.1. Energy-dispersive X-ray spectroscopy and element mapping

The results of X-ray energy dispersive spectroscopy showed that the powder synthesized without the addition of titanyl nitrate TiO(NO$_3$)$_2$ contains 3 main elements Pr, Fe, and O with the ratio Pr:Fe = 49.9:50.1 at%. Thus, the obtained sample corresponds in chemical composition to pure praseodymium orthoferrite (Fig. 1a). Powders synthesized with the addition of TiO(NO$_3$)$_2$, in terms of the ratio of key elements (Pr and Fe), also correspond to praseodymium orthoferrite within deviations of 0.1-0.6 at%, and additionally, contain titanium in the amount specified during the synthesis.

For the sample with the highest TiO$_2$ content (7.5%), energy dispersive elemental mapping was additionally carried out (Fig. 1 b-f). According to the multi-element image (Fig. 1b), the obtained sample is characterized by a uniform distribution of the key elements Ti, Fe, O, and Pr. Single-element images (Fig. 1 c-f) confirm the absence of regions enriched in individual chemical elements in the sample.

3.2. Powder X-ray diffraction

To determine the phase composition of the synthesized samples, powder X-ray diffraction was carried out, the results of which are shown in Fig. 2a. According to the obtained X-ray diffraction patterns, the reference sample (TiO$_2$-0%) is a phase-pure crystalline praseodymium orthoferrite with an orthorhombic structure. The position of the diffraction lines and their intensity are fully consistent with the known data on the structure of PrFeO$_3$ (JCPDS No: 18-9725).
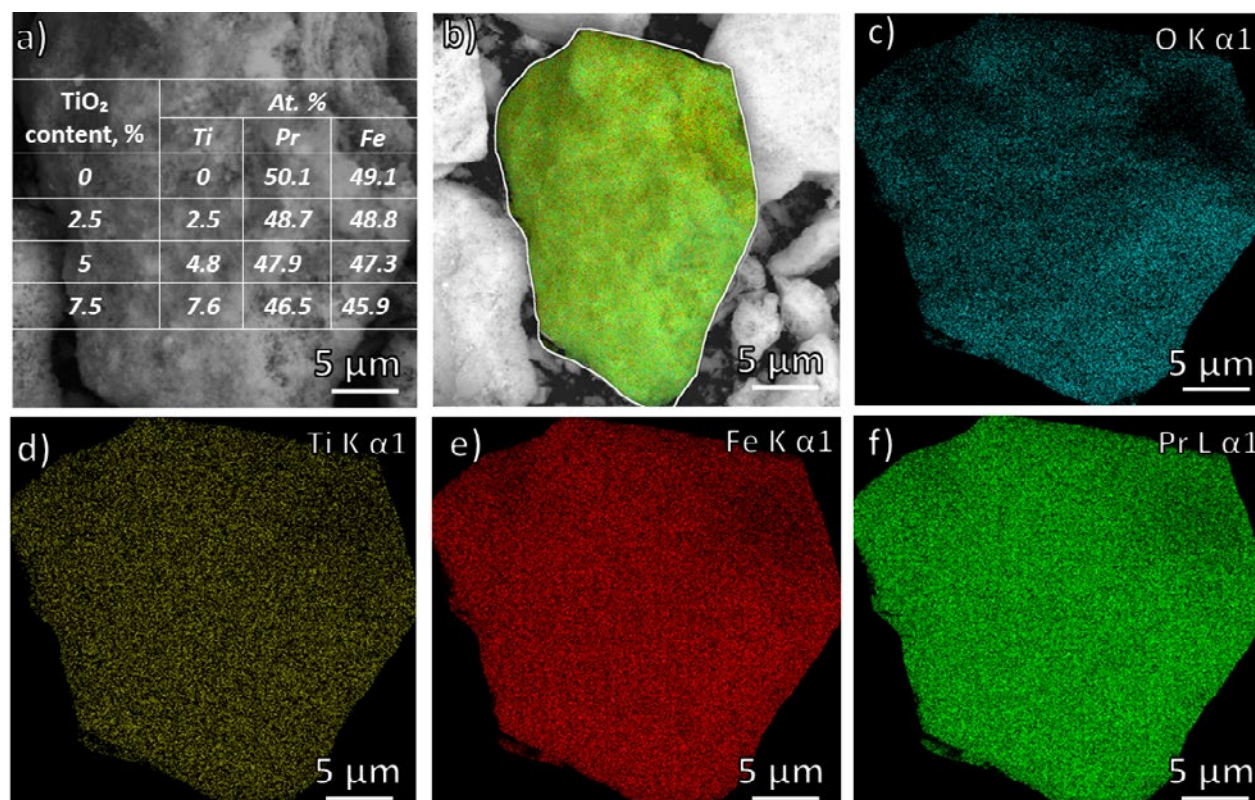
Condensed Matter and Interphases / Конденсированные среды и межфазные границы   2021;23(4): 548–560

A. S. Seroglazova et al.   Synthesis, structure, and photo-Fenton activity of PrFeO$_3$-TiO$_2$...

Fig. 1. EDS results (a) and EDS multi-element (a) and single element (c – O, d – Ti, e – Fe, f – Pr) mapping of the PrFeO$_3$-TiO$_2$-7.5% sample

The observed X-ray reflections of the samples with 2.5%, 5%, and 7.5% TiO$_2$ content also relate to orthorhombic praseodymium orthoferrite. The most intense PrFeO$_3$ X-ray diffraction lines do not have a noticeable shift, which indicates the absence of titanium being incorporated into the structure of praseodymium orthoferrite and the separate existence of the corresponding TiO$_2$ and PrFeO$_3$ phases. However, it should be noted, that there are no additional reflections in all diffractograms that could be attributed to other structural forms of TiO$_2$, which indirectly indicates its presence in an amorphous or ultradispersed (with crystallite sizes less than 5 nm) state. An increase in the TiO$_2$ content in this nanocomposite from 2.5% to 7.5% leads to a noticeable broadening of the PrFeO$_3$ diffraction lines (Fig. 2b), which indicates a decrease in the crystallite size in the series TiO$_2$-0 > TiO$_2$-2.5 > TiO$_2$-5 > TiO$_2$-7.5. The calculation of the average crystallite size of praseodymium orthoferrite confirms its decrease in this series from 47.2 nm (pure PrFeO$_3$) to 28.5 nm (TiO$_2$ content of 7.5%) (Fig. 2c). As previously shown in [25,26], such

a decrease in the crystallite size is associated with the effect of the second TiO$_2$ phase on the mass transfer processes, which complicates the recrystallization of praseodymium orthoferrite during the thermal treatment of solution combustion products.

3.3. Raman spectroscopy

To study the structural features of the TiO$_2$ and PrFeO$_3$ phases in the obtained nanocomposites, Raman spectroscopy was performed (Fig. 3). The results of the study showed the presence of combination modes belonging to titanium oxide with an anatase structure with the space group D4h19 (1$_4$/amd) [32]. The most intense peak of the Raman scattering of TiO$_2$ at 145 cm^{-1} corresponds to the E$_g$ mode. The less intense is at 197 cm^{-1} and is attributed also to the E$_g$ mode. The other modes A$_g$ – 285.8 cm^{-1}, B$_{3g}$ – 330.6 cm^{-1}, B$_{2g}$ – 428 cm^{-1}, A$_g$ - 447.8 cm^{-1}, B$_{3g}$ – 647.9 cm^{-1} confirm the formation of the PrFeO$_3$ phase with the space group Pbnm [33].

The data obtained indicate the co-existence of two separate phases: orthorhombic PrFeO$_3$
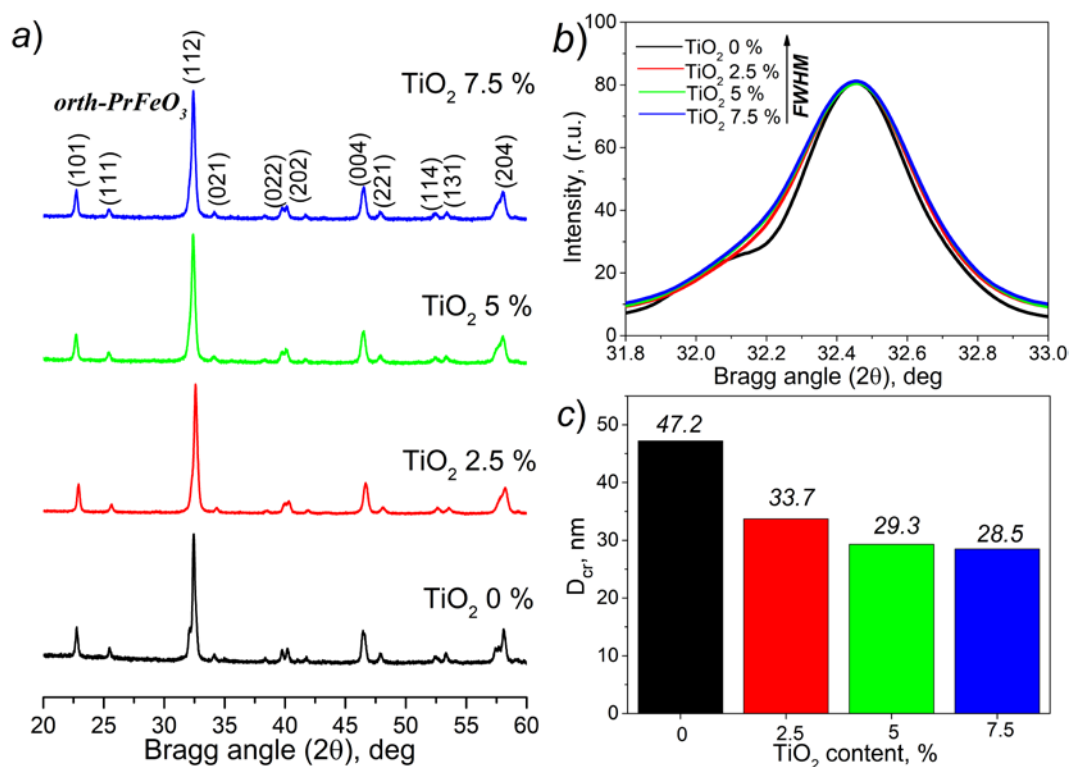
Condensed Matter and Interphases / Конденсированные среды и межфазные границы   2021;23(4): 548–560

A. S. Seroglazova et al.   Synthesis, structure, and photo-Fenton activity of PrFeO$_3$-TiO$_2$...

Fig. 2. PXRD patterns of the PrFeO$_3$-TiO$_2$ (0–7.5%) samples (a); FWHM of main (112) X-ray reflex of PrFeO$_3$ as a function of the TiO$_2$ content (b); average crystallite size of PrFeO$_3$ (c)
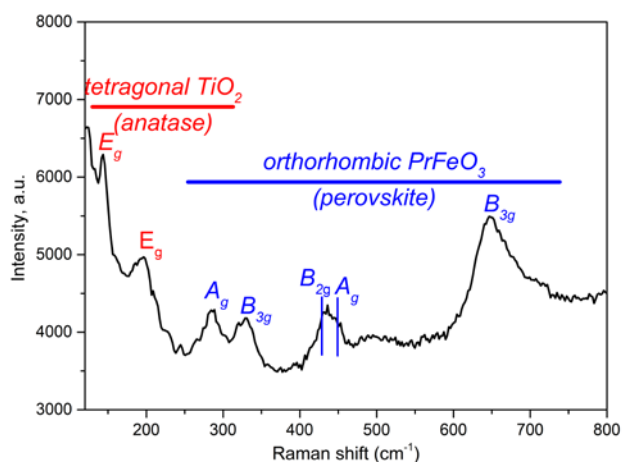

Fig. 3. Raman spectrum of the PrFeO$_3$–TiO$_2$-7.5% nanocomposite

with a perovskite structure and tetragonal TiO$_2$ with an anatase structure, which indicates the successful synthesis of the nanocomposite. Comparing these data with the results of powder X-ray diffraction, it should be concluded that TiO$_2$ in this nanocomposite occurs in the form of ultrafine nanoparticles characterized by weak crystallinity with structural motives of anatase.

3.4. Scanning electron microscopy

The morphology of the synthesized PrFeO$_3$ and PrFeO$_3$–TiO$_2$ samples was studied by the SEM method, the results of which are presented in Fig. 4. For all the samples presented, a highly porous microstructure with a developed surface and foamy morphology is observed, which is typical for oxides of powders obtained by solution combustion [3, 18, 34, 35]. The formation of a developed porous structure is associated with the abundant release of gaseous products (CO, CO$_2$, N$_2$, NO$_2$, etc.) during the redox combustion of a glycine-nitrate mixture.

It should be noted that with an increase in the proportion of TiO$_2$ in the composition of the PrFeO$_3$–TiO$_2$ composite, a visual increase in the average pore size is observed, and their size distribution becomes less uniform. Thus, in a sample with 7.5% TiO$_2$ content, pores with a size of several microns are observed, while pure PrFeO$_3$ is characterized mainly by submicron pores. In all the cases, no individual nanocrystals are observed; they are strongly aggregated into large formations (more than ten microns in size) and occupy the interpore space of the composites.
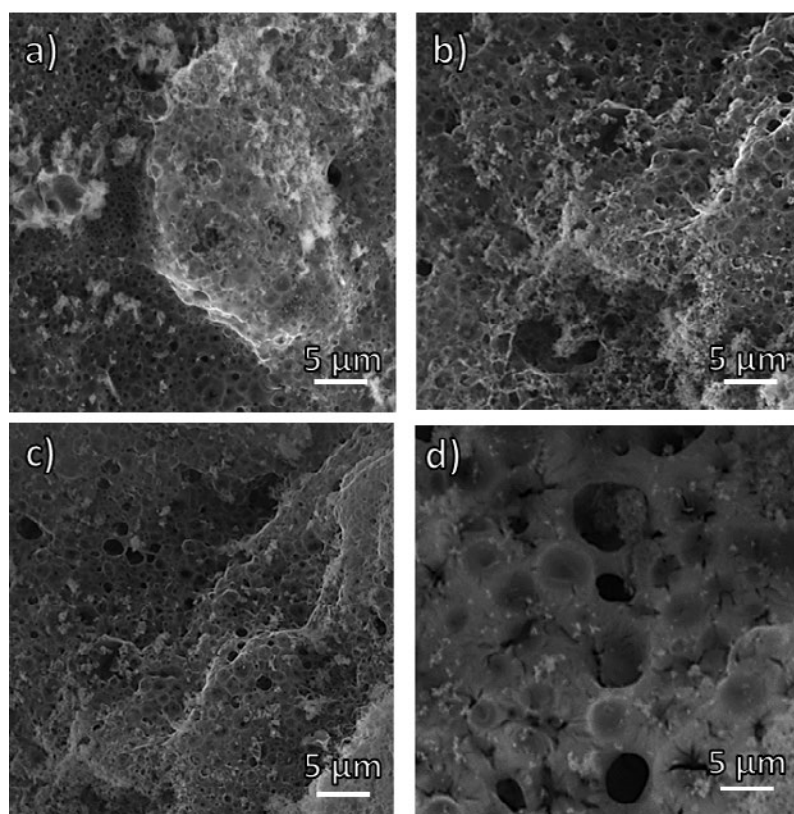
Condensed Matter and Interphases / Конденсированные среды и межфазные границы   2021;23(4): 548–560

A. S. Seroglazova et al.   Synthesis, structure, and photo-Fenton activity of PrFeO₃-TiO₂...

Fig. 4. SEM images of the PrFeO$_3$–TiO$_2$ nanocomposites synthesized at 0 (a), 2.5 (b), 5 (c) and 7.5 (d) % of TiO$_2$ content

3.5. Low-temperature nitrogen adsorption-desorption

A more detailed study of the fine porous structure of powders based on PrFeO$_3$ and TiO$_2$, as well as the determination of their specific surface area, was carried out using adsorption-structural analysis during the low-temperature (77 K) adsorption-desorption of nitrogen, the results of which are presented in Fig. 5.

According to the results obtained, all isotherms are of type II, and the hysteresis loops are of type H3, which indicates a developed meso- and macroporous structure of the obtained nanopowders with a wide pore distribution. For a pure PrFeO$_3$ sample, the smallest area of the hysteresis loop is observed, suggesting relatively low micro- and mesoporosity [29]. For samples containing the anatase TiO$_2$ phase, the area of the hysteresis loops increases with an increase in the TiO$_2$ content, which confirms an increase in porosity in this series. Based on this, it can be concluded that the addition of TiO$_2$ to PrFeO$_3$ facilitates pore formation in the composite at the stage of solution combustion of the glycine-nitrate reaction mixture.

The average pore size and specific surface area of the obtained nanocomposite powders were determined by the BJH and BET methods, respectively. According to the data presented in the inset in Fig. 5, the pure PrFeO$_3$ sample has the smallest pore size (7.2 nm) and a specific surface area of 7.6 m^2/g. For samples with variable TiO$_2$ content, the pore size and specific surface area increase in the following sequence: 5% > 7.5% > 2.5%. For TiO$_2$-2.5, these values were 10.3 nm and 13 m^2/g, for TiO$_2$-5 they were 15.2 nm and 17.8 m^2/g, and for TiO$_2$-7.5 they were 11.2 nm and 17.7 m^2/g. Earlier, it was shown [25] that, in similar cases, an increase in the average pore size and specific surface area while transforming into the composite could be associated with both suppressions of the growth of crystals of the main phase (PrFeO$_3$) and a higher specific surface area of the secondary phase (TiO$_2$), the portion of which is growing. However, with an increase in the second fraction content to 7.5%, the growth of the specific surface area and the average pore size stops, which is explained by the intensification of aggregation processes and the blocking of some of the pores by TiO$_2$ particles [36].
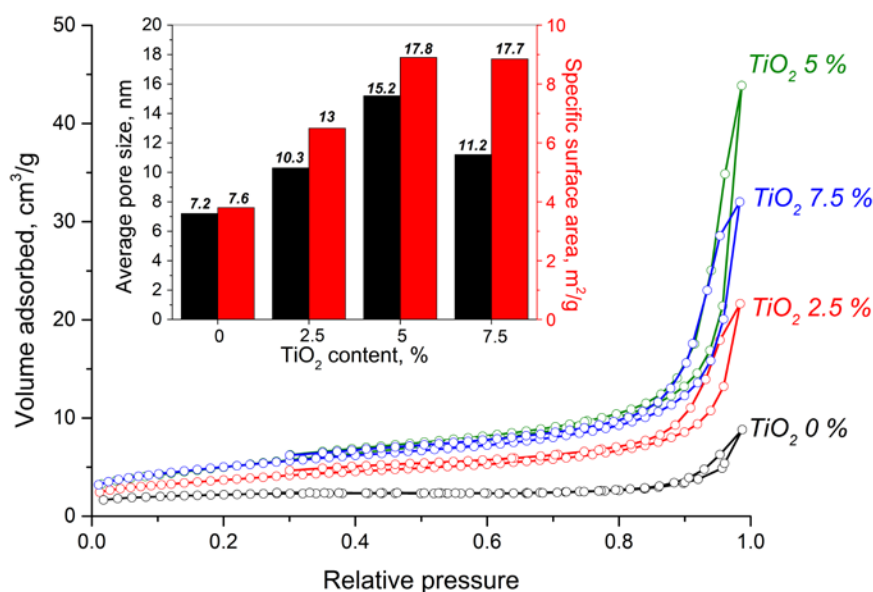
Condensed Matter and Interphases / Конденсированные среды и межфазные границы   2021;23(4): 548–560

A. S. Seroglazova et al.   Synthesis, structure, and photo-Fenton activity of PrFeO$_3$-TiO$_2$...

Fig. 5. N$_2$ adsorption-desorption isotherms of PrFeO$_3$-TiO$_2$ nanocomposites depending on the TiO$_2$ content. The inset shows the specific surface area and average pore size of the samples

3.6. UV-visible diffusion reflectance spectroscopy

To determine the edge of the optical absorption band and the band gap of the obtained PrFeO$_3$-TiO$_2$ nanocomposite powders, as well as pure PrFeO$_3$, diffusion reflection spectroscopy (DRS) in the UV-visible region was carried out (Fig. 6).

According to the DRS presented in Fig. 6a, the prepared samples are characterized by a broad absorption band from 500 to 800 nm, corresponding to the visible region of radiation. The edge of the absorption band for pure PrFeO$_3$ is in the region of slightly longer wavelengths than for PrFeO$_3$-TiO$_2$ nanocomposites and slowly decreases in the following sequence: TiO$_2$-5% > TiO$_2$-7.5% > TiO$_2$-2.5%.

To determine the band gap, Tauc plots were plotted using the transformation to the Kubelka-Munk function for the optical absorption spectra of the samples (Fig. 6b). The values of the band gap were determined from the tangent lines of the dependences concerning the photon energy [27, 37]. For pure praseodymium orthoferrite, the band gap was 2.11 eV, which is in good agreement with the results of previous studies [10, 38]. For the samples containing the anatase phase, an insignificant increase in the band gap values from 2.11 eV to 2.26 eV was observed; however, this delta is within the analysis error and the method for determining this value. Since in the case of the incorporation of titanium into the structure of

praseodymium orthoferrite, a significant change in the value of E_g would be observed, and in our case, it can be neglected, the results obtained are in good agreement with the data of PXRD and Raman spectroscopy, once again confirming the co-existence of the PrFeO$_3$ and TiO$_2$ phases in the nanocomposite in the form of separate phases.

3.7. Fenton-like catalytic activity analysis

Based on the results of SEM, adsorption-structural analysis, and DRS, it was concluded that the obtained PrFeO$_3$ and PrFeO$_3$–TiO$_2$ powders could be promising photocatalysts. Therefore, their functional properties were investigated in the photocatalytic process of Fenton-like oxidation of methyl violet under the action of visible light. The results of these studies are shown in Fig. 7.

Fig. 7a contains the typical absorption spectra of a methyl violet solution after a survey photocatalytic test with PrFeO$_3$ and PrFeO$_3$–TiO$_2$ nanopowders. It follows from these results that the PrFeO$_3$-TiO$_2$-5% sample has the highest catalytic activity, for which, according to the results of low-temperature adsorption analysis, the highest values of the specific surface area and average pore size (17.8 m^2/g and 15.2 nm) have been established. A higher activity, in this case, is achieved due to higher accessibility of the surface, the increased total number of active centers, easier access of reagents, and removal
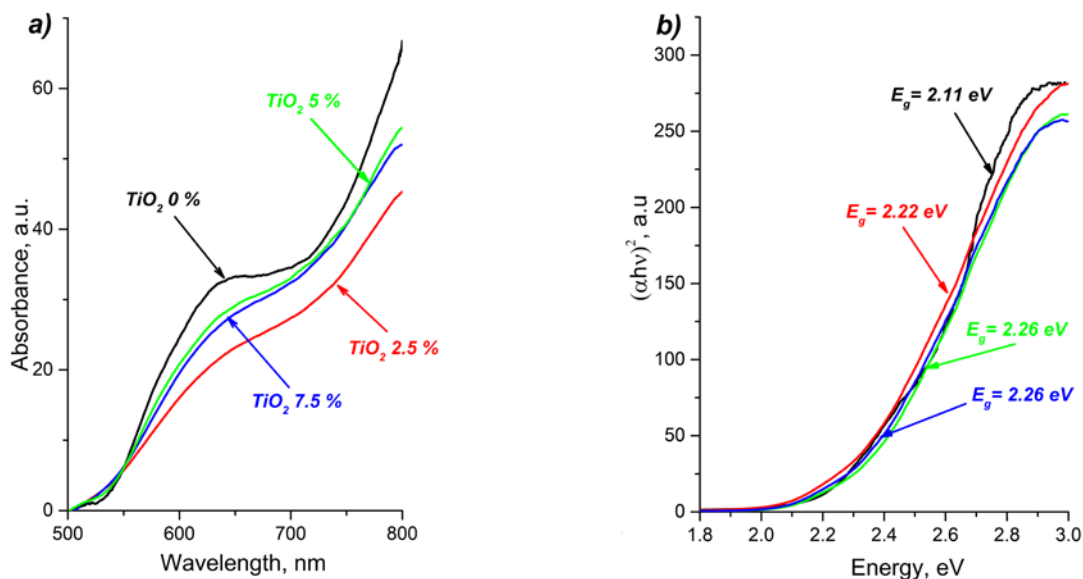
Condensed Matter and Interphases / Конденсированные среды и межфазные границы   2021;23(4): 548–560

A. S. Seroglazova et al.   Synthesis, structure, and photo-Fenton activity of PrFeO₃-TiO₂...

Fig. 6. UV-visible diffusion reflectance spectra of $PrFeO_3$ and $PrFeO_3$–TiO_2 samples (a) and corresponding Tauc plots (b)

of reaction products from the pore structure of the nanocomposite [23–25]. However, the nanocomposite photocatalyst $PrFeO_3$–TiO_2-7.5%, which has a higher specific surface area and average pore size (17.7 m^2/g and 11.2 nm) compared to the $PrFeO_3$ and $PrFeO_3$–TiO_2-2.5% samples, exhibits the lowest photocatalytic activity among them. In this case, a decrease in the efficiency of dye removal may be associated

with a decrease in the efficiency of radiation absorption by photoactive $PrFeO_3$ due to its shielding by TiO_2 particles located on the surface of large $PrFeO_3$ particles (Fig. 8). Nevertheless, the process of generation of oxidative radicals from water molecules ($H_2O \rightarrow \cdot OH$) during the photo-Fenton-like reaction (Fig. 8) can be suppressed, which was previously reported [21, 39]. In this case, an increase in the photocatalytic
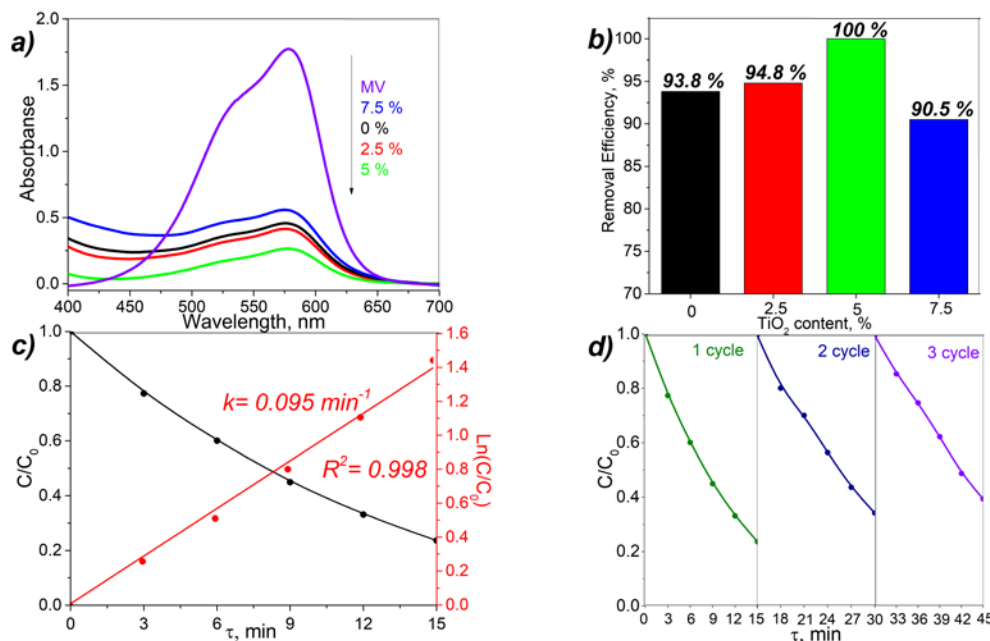

Fig. 7. UV-visible absorption spectra of MV dye during photo-Fenton-like oxidation (a); removal efficiency of $PrFeO_3$ and $PrFeO_3$-TiO_2 nanopowders depending on the TiO_2 content (b); MV concentration and kinetic curves of the $PrFeO_3$-TiO_2-5% sample (c)

Condensed Matter and Interphases / Конденсированные среды и межфазные границы   2021;23(4): 548–560

A. S. Seroglazova et al.   Synthesis, structure, and photo-Fenton activity of PrFeO$_3$-TiO$_2$...

activity of nanopowders based on praseodymium orthoferrite and the addition of titanium dioxide is provided by the formation of a heterojunction, which allows charge carriers to transfer to the second phase and thereby reduce the negative effect of reverse recombination of electron-hole pairs [19]. Thus, the catalytic activity of the samples decreases in the sequence TiO$_2$-5% > TiO$_2$-2.5% > TiO$_2$-0% > TiO$_2$-7.5% and the optimum positive effect of the introduction of TiO$_2$ on the photocatalytic activity of the nanocomposite is observed in the TiO$_2$-5% sample.

For the PrFeO$_3$–TiO$_2$-5% sample, providing 100% MV photodegradation under previously indicated experimental conditions, kinetic studies were carried out and the results obtained are presented in Fig. 7c. As the irradiation time of the solution increases, the relative concentration of the dye naturally decreases, and the kinetic dependence corresponds to the pseudo-first-order of the reaction. The rate constant of this process was calculated based on the linearization of the kinetic dependence in logarithmic coordinates and amounted to 0.095 min^{-1}. When comparing the results obtained with the results of photocatalytic tests of other nanocrystalline orthoferrites (Table 1), it was shown that the PrFeO$_3$–TiO$_2$-5% sample is superior to the best analogs known.

A prerequisite for the further practical application of photocatalysts is their high stability and cyclic reproducibility of results. The study of the cyclic photodegradation of the MV dye by visible light in the presence of PrFeO$_3$-TiO$_2$-5% was carried out under the same conditions as the kinetic study. The results of the cyclic stability experiment (Fig. 7d) indicate that after three cycles of the methyl violet
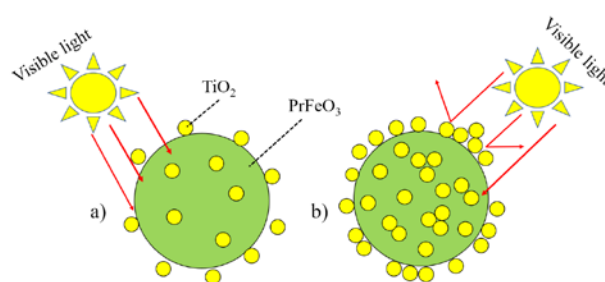

Fig. 8. Schematic representation of PrFeO$_3$ shielding effect by TiO$_2$ particles upon absorption of visible light by the nanocomposite with low (a) and high (b) TiO$_2$ content

photodegradation process, there is only a slight loss of photocatalytic activity, which confirms its high stability of functioning under the selected conditions. This insignificant decrease in photocatalytic activity may be due to the physical loss of the catalyst during its separation from the initial solution. The amount of catalytic testing results makes it possible to consider PrFeO$_3$–TiO$_2$ nanocomposite powders as a promising basis for the processes of photo-Fenton-like oxidation of organic pollutants in aqueous media.

4. Conclusion

In the current study, the method of glycine-nitrate combustion followed by heat treatment in the air has been successfully applied to obtain nanocomposite porous materials based on PrFeO$_3$–TiO$_2$ with a variable mass content of TiO$_2$ (0-7.5%). It is shown that the obtained powders contain nanocrystals of orthorhombic PrFeO$_3$ and an ultradispersed TiO$_2$ phase with an anatase structure. It is revealed that the TiO$_2$ content has a significant effect on the average crystallite size, the specific surface area, and the average pore volume of the samples, which at the considered

Table 1. Photocatalytic characteristics comparison of the PrFeO$_3$–TiO$_2$-5% nanocomposite photocatalyst with other orthoferrite-based photocatalysts described in the literature

№	Photocatalyst	Synthesis method	Band gap, eV	Lamp	Pollutant	K, min^{-1}	Ref.
1	EuFeO$_3$ nanoparticles	Sol-gel	2.22	Xenon	Rhodamine B	0.002	[23]
2	YbFeO$_3$ nanopowder	Solution-combustion	2.05	LED	Methyl violet	0.004	[19]
3	BiFeO$_3$ nanopowder	Sol-gel	2.21	Sunlight	Mordant blue	0.009	[40]
4	PrFeO$_3$-TiO$_2$-5% nanocomposite	Solution-combustion	2.22	Xenon	Methyl violet	0.095	This work

Condensed Matter and Interphases / Конденсированные среды и межфазные границы   2021;23(4): 548–560

A. S. Seroglazova et al.   Synthesis, structure, and photo-Fenton activity of $PrFeO_3$-TiO_2...

concentrations suppresses the growth of $PrFeO_3$ nanocrystals and increases the total porosity of the nanocomposite. The amount of added TiO_2 has practically no effect on the band gap values, which confirms the formation of $PrFeO_3$-TiO_2 composite consisting of two independent phases. The photocatalytic activity of the synthesized nanocomposite samples has been studied in Fenton-like oxidation of methyl violet. The optimal TiO_2 content in the nanocomposite is 5 wt%, which ensures the 100% removal of methyl violet from an aqueous solution. Compared to pure catalysts based on other orthoferrites, the $PrFeO_3$-TiO_2 nanocomposites obtained in this work exhibit higher photocatalytic activity. Thus, the resulting nanopowders are promising photocatalysts for modern wastewater treatment processes.

Author contribution

All authors made an equivalent contribution to the preparation of the publication.

Conflict of interests

The authors declare that they have no known competing financial interests or personal relationships that could have influenced the work reported in this paper.

References

1. Zhou Z., Guo L., Yang H., Liu Q., Ye F. Hydrothermal synthesis and magnetic properties of multiferroic rare-earth orthoferrites. *Journal of Alloys and Compounds*. 2014;583: 21–31. https://doi.org/10.1016/j.jallcom.2013.08.129

2. Lü X., Xie J., Shu H., Liu J., Yin C., Lin J. Microwave-assisted synthesis of nanocrystalline $YFeO_3$ and study of its photoactivity. *Materials Science and Engineering B: Solid-State Materials for Advanced Technology*. 2007;138(3): 289–292. https://doi.org/10.1016/j.mseb.2007.01.003

3. Martinson K. D., Ivanov V. A., Chebanenko M. I., Panchuk V. V., Semenov V. G., Popkov V. I. Facile combustion synthesis of $TbFeO_3$ nanocrystals with hexagonal and orthorhombic structure. *Nanosystems: Physics, Chemistry, Mathematics*. 2019;10(6): 694–700. https://doi.org/10.17586/2220-8054-2019-10-6-694-700

4. Ding J., Lü X., Shu H., Xie J., Zhang H. Microwave-assisted synthesis of perovskite $ReFeO_3$ (Re: La, Sm, Eu, Gd) photocatalyst. *Materials Science and Engineering B: Solid-State Materials for Advanced Technology*. 2010;171(1-3): 31–34. https://doi.org/10.1016/j.mseb.2010.03.050

5. Nguyen A. T., Nguyen N. T., Mittova I. Y., Perov N. S., Mittova V. O., Hoang T. C., Nguyen V. M., Nguyen V. H., Pham V., Bui X. V. Crystal structure, optical and magnetic properties of $PrFeO_3$ nanoparticles prepared by modified co-precipitation method. *Processing and Application of Ceramics*. 2020;14(4): 355-361. https://doi.org/10.2298/PAC2004355N

6. Akbashev A. R., Semisalova A. S., Perov N. S., Kaul A. R. Weak ferromagnetism in hexagonal orthoferrites $RFeO_3$ (R = Lu, Er-Tb). *Applied Physics Letters*. 2011;99(12): 2011–2014. https://doi.org/10.1063/1.3643043

7. Tugova E., Yastrebov S., Karpov O., Smith R. $NdFeO_3$ nanocrystals under glycine nitrate combustion formation. *Journal of Crystal Growth*. 2017;467: 88–92. https://doi.org/10.1016/j.jcrysgro.2017.03.022

8. Martinson K. D., Kondrashkova I. S., Omarov S. O., Sladkovskiy D. A., Kiselev A. S., Kiseleva T. Y., Popkov V. I. Magnetically recoverable catalyst based on porous nanocrystalline $HoFeO_3$ for processes of n-hexane conversion. *Advanced Powder Technology*. 2020;31(1): 402–408. https://doi.org/10.1016/j.apt.2019.10.033

9. Nguyen A. T., Nguyen V. Y., Mittova I. Ya., Mittova V. O., Viryutina E. L., Hoang C. Ch. T., Nguyen Tr. L. T., Bui X. V., Do T. H. Synthesis and magnetic properties of $PrFeO_3$ nanopowders by the co-precipitation method using ethanol. *Nanosystems: Physics, Chemistry, Mathematics*. 2020;11(4): 468–473. https://doi.org/10.17586/2220-8054-2020-11-4-468-473

10. Li L., Zhang M., Tian P., Gu W., Wang X. Synergistic photocatalytic activity of $LnFeO_3$ (Ln=Pr, Y) perovskites under visible light illumination. *Ceramics International*. 2014;40(9): 13813–13817. https://doi.org/10.1016/j.ceramint.2014.05.097

11. Freeman E., Kumar S., Thomas S. R., Pickering H., Fermin D. J., Eslava S. $PrFeO_3$ photocathodes prepared through spray pyrolysis. *ChemElectroChem*. 2020;7(6): 1365–1372. https://doi.org/10.1002/celc.201902005

12. Tang P., Xie X., Chen H., Lv C., Ding Y. Synthesis of nanoparticulate $PrFeO_3$ by sol-gel method and its visible-light photocatalytic activity. *Ferroelectrics*. 2019;546(1): 181–187. https://doi.org/10.1080/00150193.2019.1592470

13. Qin C., Li Z., Chen G., Zhao Y., Lin T. Fabrication and visible-light photocatalytic behavior of perovskite praseodymium ferrite porous nanotubes. *Journal of Power Sources*. 2015;285: 178–184. https://doi.org/10.1016/j.jpowsour.2015.03.096

14. Thirumalairajan S., Girija K., Ganesh I., Mangalaraj D., Viswanathan C., Balamurugan A., Ponpandian N. Controlled synthesis of perovskite $LaFeO_3$ microsphere composed of nanoparticles via self-as-

Condensed Matter and Interphases / Конденсированные среды и межфазные границы   2021;23(4): 548–560

A. S. Seroglazova et al.   Synthesis, structure, and photo-Fenton activity of PrFeO$_3$-TiO$_2$...

sembly process and their associated photocatalytic activity. *Chemical Engineering Journal*. 2012;209: 420–428. https://doi.org/10.1016/j.cej.2012.08.012

15. Rusevova K., Köferstein R., Rosell M., Richnow H. H., Kopinke F. D., Georgi A. LaFeO$_3$ and BiFeO$_3$ perovskites as nanocatalysts for contaminant degradation in heterogeneous Fenton-like reactions. *Chemical Engineering Journal*. 2014;239: 322–331. https://doi.org/10.1016/j.cej.2013.11.025

16. Kondrashkova I. S., Martinson K. D., Zakharova N. V., Popkov V. I. Synthesis of nanocrystalline HoFeO$_3$ photocatalyst via heat treatment of products of glycine-nitrate combustion. *Russian Journal of General Chemistry*. 2018;88(12): 2465–2471. https://doi.org/10.1134/S1070363218120022

17. Wen W., Wu J. M. Nanomaterials via solution combustion synthesis: A step nearer to controllability. *RSC Advances*. 2014;4(101): 58090–58100. https://doi.org/10.1039/c4ra10145f

18. Popkov V. I., Martinson K. D., Kondrashkova I. S., Enikeeva M. O., Nevedomskiy V. N., Panchuk V. V., Semenov V. G., Volkov M. P., Pleshakov I. V. SCS-assisted production of EuFeO$_3$ core-shell nanoparticles: formation process, structural features and magnetic behavior. *Journal of Alloys and Compounds*. 2021;859: 157812. https://doi.org/10.1016/j.jallcom.2020.157812

19. Tikhanova S. M., Lebedev L. A., Martinson K. D., Chebanenko M. I., Buryanenko I. V., Semenov V. G., Nevedomskiy V. N., Popkov V. I. Synthesis of novel heterojunction h-YbFeO$_3$/o-YbFeO$_3$ photocatalyst with enhanced Fenton-like activity under visible-light. *New Journal of Chemistry*. 2021;45(3): 1541–1550. https://doi.org/10.1039/D0NJ04895J

20. Mir F. A., Sharma S. K., Kumar R. Magnetizations and magneto-transport properties of Ni-doped PrFeO$_3$ thin films. *Chinese Physics B*. 2014;23(4): 048101. https://doi.org/10.1088/1674-1056/23/4/048101

21. Rehman F., Sayed M., Khan J. A., Shah L. A., Shah N. S., Khan H. M., Khattak R. Degradation of crystal violet dye by fenton and photo-fenton oxidation processes. *Zeitschrift Fur Physikalische Chemie*. 2018;232(12): 1771–1786. https://doi.org/10.1515/zpch-2017-1099

22. . Luo W, Zhu L., Wang N., Tang H., Cao M., She Y. Efficient removal of organic pollutants with magnetic nanoscaled BiFeO$_3$ as a reusable heterogeneous Fenton-like catalyst. *Environmental Science and Technology*. 2010;44(5): 1786–1791. https://doi.org/10.1021/es903390g

23. Ju L., Chen Z., Fang L., Dong W., Zheng F., Shen M. Sol-gel synthesis and photo-Fenton-like catalytic activity of EuFeO$_3$ nanoparticles. *Journal of the American Ceramic Society*. 2011;94(10): 3418–3424. https://doi.org/10.1111/j.1551-2916.2011.04522.x

24. Shi S., Xu J., Li L. Preparation and photocatalytic activity of ZnO nanorods and ZnO/Cu$_2$O nanocomposites. *Main Group Chemistry*. 2017;16(1): 47–55. https://doi.org/10.3233/MGC-160224

25. Kim J. Y., Kang S. H., Kim H. S., Sung Y. E. Preparation of highly ordered mesoporous Al$_2$O$_3$/TiO$_2$ and its application in dye-sensitized solar cells. *Langmuir*. 2010;26(4): 2864–2870. https://doi.org/10.1021/la902931w

26. Cam T. S., Vishnevskaya T. A., Omarov S. O., Nevedomskiy V. N., Popkov V. I., Urea–nitrate combustion synthesis of CuO/CeO$_2$ nanocatalysts toward low-temperature oxidation of CO: the effect of Red/Ox ratio. *Journal of Materials Science*. 2020;55(26): 11891–11906. https://doi.org/10.1007/s10853-020-04857-3

27. Faisal M., Harraz F. A., Ismail A. A., El-Toni A. M., Al-Sayari S. A., Al-Hajry A., Al-Assiri M. S. Novel mesoporous NiO/TiO$_2$ nanocomposites with enhanced photocatalytic activity under visible light illumination. *Ceramics International*. 2018;44(6): 7047–7056. https://doi.org/10.1016/j.ceramint.2018.01.140

28. Mu J., Chen B., Zhang M., Guo Z., Zhang P., Zhang Z., Sun Y., Shao C., Liu Y. Enhancement of the visible-light photocatalytic activity of In$_2$O$_3$-TiO$_2$ nanofiber heteroarchitectures. *ACS Applied Materials & Interfaces*. 2012;4(1): 424–430. https://doi.org/10.1021/am201499r

29. Yu H., Yu J., Cheng B. Photocatalytic activity of the calcined H-titanate nanowires for photocatalytic oxidation of acetone in air. *Chemosphere*. 2007;66(11): 2050–2057. https://doi.org/10.1016/j.chemosphere.2006.09.080

30. Boulbar E. Le, Millon E., Cachoncinlle C., Hakim B., Ntsoenzok E. Optical properties of rare-earth-doped TiO$_2$ anatase and rutile thin films grown by pulsed-laser deposition. *Thin Solid Films*. 2013;553: 13–16. https://doi.org/10.1016/j.tsf.2013.11.032

31. Ismail A. A., Bahnemann D. W. Mesoporous titania photocatalysts: Preparation, characterization and reaction mechanisms. *Journal of Materials Chemistry*. 2011;21(32): 11686–11707. https://doi.org/10.1039/c1jm10407a

32. Yadav H. M., Kolekar T. V., Barge A. S., Thorat N. D., Delekar S. D., Kim B. M., Kim B. J., Kim J. S. Enhanced visible-light photocatalytic activity of Cr^{3+}-doped anatase TiO$_2$ nanoparticles synthesized by sol-gel method. *Journal of Materials Science: Materials in Electronics*. 2015;27(1): 526-534. https://doi.org/10.1007/s10854-015-3785-6

33. Rozenberg G. K., Pasternak M. P., Xu W. M., Dubrovinsky L. S., Carlson S., Taylor R. D. Consequences of pressure-instigated spin crossover in RFeO$_3$ perovskites; a volume collapse with no symmetry modification. *Europhysics Letters*. 2005;71(2): 228–234. https://doi.org/10.1209/epl/i2005-10071-9

Condensed Matter and Interphases / Конденсированные среды и межфазные границы   2021;23(4): 548–560

A. S. Seroglazova et al.   Synthesis, structure, and photo-Fenton activity of PrFeO$_3$-TiO$_2$...

34. Kotlovanova N. E., Matveeva A. N., Omarov S. O., Sokolov V. V., Akbaeva D. N., Popkov V. I. Formation and acid-base surface properties of highly dispersed η-Al$_2$O$_3$ nanopowders. *Inorganic Materials*. 2018;54(4): 392–400. https://doi.org/10.1134/S0020168518040052

35. Khaliullin S. M., Zhuravlev V. D., Ermakova L. V., Buldakova L. Y., Yanchenko M. Y., Porotnikova N. M. Solution combustion synthesis of ZnO using binary fuel (glycine + citric acid). *International Journal of Self-Propagating High-Temperature Synthesis*. 2019;28(4): 226–232. https://doi.org/10.3103/S1061386219040058

36. Ismail A. A., Robben L., Bahnemann D. W. Study of the efficiency of UV and visible-light photocatalytic oxidation of methanol on mesoporous RuO$_2$-TiO$_2$ nanocomposites. *ChemPhysChem*. 2011;12(5): 982–991. https://doi.org/10.1002/cphc.201000936

37. Peymani-Motlagh S. M., Sobhani-Nasab A., Rostami M., Sobati H., Eghbali-Arani M., Fasihi-Ramandi M., Ganjali M. R., Rahimi-Nasrabadi M. Assessing the magnetic, cytotoxic and photocatalytic influence of incorporating Yb^{3+} or Pr^{3+} ions in cobalt-nickel ferrite. *Journal of Materials Science: Materials in Electronics*. 2019;30(7): 6902–6909. https://doi.org/10.1007/s10854-019-01005-9

38. Abdellahi M., Abhari A. S., Bahmanpour M. Preparation and characterization of orthoferrite PrFeO$_3$ nanoceramic. *Ceramics International*. 2016;42(4): 4637–4641. https://doi.org/10.1016/j.ceramint.2015.12.027

39. Goldstein S., Meyerstein D. Comments: on the mechanism of the Fenton-like reaction. *Accounts of Chemical Research*. 1999;32(7): 547–550. https://doi.org/10.1021/ar9800789

40. Ćirković J., Radojković A., Luković Golić D., Tasić N., Čizmić M., Branković G., Branković Z. Visible-light photocatalytic degradation of Mordant Blue 9 by single-phase BiFeO$_3$ nanoparticles. *Journal of Environmental Chemical Engineering*. 2021;9(1): 104587. https://doi.org/10.1016/j.jece.2020.104587

Information about the authors

Anna S. Seroglazova, student at the Departament of Physical Chemistry, Saint Petersburg State Technological Institute (University), Russian Federation. Laboratory assistent, Ioffe Physical-Technical Institute of the Russian Academy of Sciences, Russian Federation; e-mail: annaseroglazova@yandex.ru. ORCID: https://orcid.org/0000-0002-3304-9068.

Maria I. Chebanenko, Junior Researcher at the Laboratory of Materials and Processes of Hydrogen Energy, Ioffe Physical-Technical Institute of the Russian Academy of Sciences, Russian Federation; e-mail: m_chebanenko@list.ru. ORCID: https://orcid.org/0000-0002-1461-579X.

Vadim I. Popkov, PhD in Chemistry, Senior Research Fellow, Head of the Laboratory of Materials and Processes of Hydrogen Energy, Ioffe Physical-Technical Institute of the Russian Academy of Sciences, Russian Federation; e-mail: vip-07@yandex.ru. ORCID: https://orcid.org/0000-0002-8450-4278.